ARTICLES
https://doi.org/10.1038/s41591-018-0032-8

nature medicine

An immune-beige adipocyte communication via nicotinic acetylcholine receptor signaling

Heejin Jun[1], Hui Yu[1,2], Jianke Gong[1,3], Juan Jiang[1,4], Xiaona Qiao[1,5], Eric Perkey[6,7,8], Dong-il Kim[1], Margo P. Emont[1,2], Alexander G. Zestos[9,13], Jung-Sun Cho[1], Jianfeng Liu[3], Robert T. Kennedy[9,10], Ivan Maillard[1,7,11,12,14], X. Z. Shawn Xu[1,2] and Jun Wu[1,2]*

Beige adipocytes have recently been shown to regulate energy dissipation when activated and help organisms defend against hypothermia and obesity. Prior reports indicate that beige-like adipocytes exist in adult humans and that they may present novel opportunities to curb the global epidemic in obesity and metabolic illnesses. In an effort to identify unique features of activated beige adipocytes, we found that expression of the cholinergic receptor nicotinic alpha 2 subunit (*Chrna2*) was induced in subcutaneous fat during the activation of these cells and that acetylcholine-producing immune cells within this tissue regulated this signaling pathway via paracrine mechanisms. CHRNA2 functioned selectively in uncoupling protein 1 (*Ucp1*)-positive beige adipocytes, increasing thermogenesis through a cAMP- and protein kinase A-dependent pathway. Furthermore, this signaling via CHRNA2 was conserved and present in human subcutaneous adipocytes. Inactivation of *Chrna2* in mice compromised the cold-induced thermogenic response selectively in subcutaneous fat and exacerbated high-fat diet-induced obesity and associated metabolic disorders, indicating that even partial loss of beige fat regulation in vivo had detrimental consequences. Our results reveal a beige-selective immune–adipose interaction mediated through CHRNA2 and identify a novel function of nicotinic acetylcholine receptors in energy metabolism. These findings may lead to identification of therapeutic targets to counteract human obesity.

The serious metabolic complications closely associated with obesity emphasize the urgency to develop counteracting strategies. It has recently been reported that beige-like thermogenic adipocytes are present in human adults[1–4] and that the activation of these thermogenic fat cells increases energy expenditure and improves metabolic health in humans[5–9]. Whereas the regulation of white and classical brown fat cells has been investigated for decades, many aspects of the beige adipocyte function are still yet to be elucidated.

Previous studies of the regulation of thermogenic fat cells in vivo have mainly been focused on signaling through the β-adrenergic pathway[10]. Here we demonstrate that expression of CHRNA2, a subunit of the nicotinic acetylcholine receptor (nAChR) family, is upregulated during beiging and that it specifically functions in beige fat cells from subcutaneous adipose depots. The nACHRs belong to a large superfamily of ligand-gated ion channels that are expressed throughout both the central and the peripheral nervous systems, as well as in non-neuronal cell populations[11,12]. At an individual-cell-level resolution, we observed that CHRNA2-mediated signaling specifically occurred in *Ucp1*-expressing beige fat cells within subcutaneous culture, but not in either white or brown fat cells. Calcium imaging assays further revealed that primary fat cells from the human subcutaneous depot, but not those from the perirenal depot, responded to stimulation with a CHRNA2 agonist, suggesting that this beige-selective response was conserved in humans. We identified acetylcholine-producing immune cells within the subcutaneous fat depot that communicated with beige fat cells via CHRNA2 through paracrine signaling. Additionally, *Chrna2*-knockout (hereafter referred to as *Chrna2* KO) mice had a compromised response to cold, specifically in beige fat, and impaired metabolic homeostasis after dietary challenges. Our results identify CHRNA2 as a functional beige-selective marker and suggest that this immune–adipose interaction through acetylcholine and CHRNA2 may lead to novel druggable targets to treat human obesity and the metabolic syndrome.

Results

***Chrna2* is induced in subcutaneous adipocytes during the process of beiging.** Rosiglitazone (Rosi), a thiazolidinedione (TZD) that acts as a peroxisome proliferator-activated receptor (PPAR)-γ agonist, has been shown to induce the activation of thermogenic fat ('browning') in vitro and in vivo[13–15]. Thus, to investigate which signaling pathways activate beige adipocytes, we performed a microarray analysis with RNA samples from fully differentiated primary

[1]Life Sciences Institute, University of Michigan, Ann Arbor, MI, USA. [2]Department of Molecular and Integrative Physiology, University of Michigan Medical School, Ann Arbor, MI, USA. [3]International Research Center for Sensory Biology and Technology of MOST, Key Laboratory of Molecular Biophysics of MOE, College of Life Science and Technology, Huazhong University of Science and Technology, Wuhan, China. [4]Department of Respiratory Medicine, Key Site of National Clinical Research Center for Respiratory Diseases, Xiangya Hospital, Central South University, Changsha, China. [5]Huashan Hospital, Fudan University, Shanghai, China. [6]Center for Stem Cell Biology, Life Sciences Institute, University of Michigan, Ann Arbor, MI, USA. [7]Graduate Program in Cellular and Molecular Biology, University of Michigan, Ann Arbor, MI, USA. [8]Medical Scientist Training Program, University of Michigan, Ann Arbor, MI, USA. [9]Department of Chemistry, University of Michigan, Ann Arbor, MI, USA. [10]Department of Pharmacology, University of Michigan, Ann Arbor, MI, USA. [11]Division of Hematology–Oncology, Department of Medicine, University of Michigan, Ann Arbor, MI, USA. [12]Department of Cell and Developmental Biology, University of Michigan, Ann Arbor, MI, USA. [13]Present address: Department of Chemistry, Center for Behavioral Neuroscience, American University, Washington, D.C., USA. [14]Present address: Division of Hematology–Oncology, Department of Medicine and Abramson Family Cancer Research Institute, University of Pennsylvania Perelman School of Medicine, Philadelphia, PA, USA. *e-mail: wujunz@umich.edu

preadipocytes that were isolated from the mouse inguinal subcutaneous fat depot (in which beige adipocytes are most abundant) and treated in vitro with either Rosi or a vehicle control. As expected, the thermogenic marker *Ucp1* was induced in the Rosi-treated samples. It is of note that *Chrna2*, which encodes one of the subunits of nAChRs, was greatly induced after Rosi treatment in these fat-cell cultures (Fig. 1a). Induction of *Chrna2* expression was confirmed by quantitative PCR (qPCR) analysis of primary inguinal fat cells from multiple strains of inbred mice (Fig. 1a and Supplementary Fig. 1a). Further analyses revealed that *Chrna2* was expressed at substantial levels in subcutaneous adipocytes that among all of the nAChR-subunit-encoding genes, it was the only one whose expression level was regulated during Rosi-induced beiging (Fig. 1b and Supplementary Fig. 1b,c).

A spectrum of signaling pathways and molecules has been reported to activate adaptive thermogenesis in adipocytes[10]. *Chrna2* expression is induced by many of these beiging stimuli, which include norepinephrine, isoproterenol (Iso; a pan-adrenergic agonist), CL-316,243 (CL; a β3-adrenergic-specific agonist), dibutyryl-cAMP (cAMP; a cyclic nucleotide derivative that mimics endogenous cAMP) and triiodothyronine (T3; a thyroid hormone that has long been known to have a role in regulating thermogenesis[10]) (Fig. 1c). Furthermore, *Chrna2* mRNA expression was induced during in vivo 'beiging' in the inguinal fat after cold exposure (CE) or Rosi treatment (Fig. 1d and Supplementary Fig. 1d). Conversely, *Chrna2* expression was substantially lower in inguinal fat of obese mice as compared to that of lean mice (Supplementary Fig. 1e). It has been previously reported that differentiated human adipose precursors from subcutaneous fat respond to thermogenic stimulants[16,17], suggesting that besides their presence in the supraclavicular region, thermogenic adipocytes may also exist in the human subcutaneous depot. Similar to their mouse counterparts, induction of *CHRNA2* expression was observed after treatments with Rosi and Iso in differentiated primary adipose stromal cells (ASCs) that were isolated from the human subcutaneous depot (Fig. 1e), indicating that this observed *Chrna2* induction is relevant to human physiology.

Mechanistic studies revealed that in addition to adipogenic and thermogenic markers, such as *Pparg* and *Ucp1*, *Chrna2* expression was markedly induced during the adipogenesis of inguinal preadipocytes after chronic Rosi treatment (Fig. 1f). A promoter fragment containing 1.1 kb of the 5′ flanking region of mouse *Chrna2* was activated (induced by fourfold) by the expression of PPAR-γ (Fig. 1g). Chromatin immunoprecipitation (ChIP) assays confirmed that PPAR-γ recruitment was enriched on the promoter region of *Chrna2*, between −164 bp and −151 bp, to stimulate *Chrna2* transcription in inguinal adipocytes (Fig. 1h). Together these data suggest that *Chrna2* is regulated by PPAR-γ as a direct target during beige adipogenesis (Supplementary Fig. 2).

CHRNA2 signaling is beige adipocyte selective. To directly examine whether CHRNA2-containing ion channels were functional in fat cells (particularly beige adipocytes, as *Chrna2* is inducible during the beiging process), we generated 'beige-fat reporter mice' by crossing *Ucp1–Cre* transgenic mice[18] with Ai14 reporter mice[19], in which *Ucp1*-expressing adipocytes are labeled with red fluorescent protein (RFP) (Fig. 2a). We validated the presence of RFP^+ cells through analysis of *Rfp* (*tdTomato*) expression in differentiated primary inguinal preadipocytes, as well as in the inguinal adipose tissue of *Ucp1–Cre–Rfp* mice (Supplementary Fig. 3). Both acetylcholine and nicotine, agonists of nAChR channels, induced an increase in intracellular calcium in the RFP-labeled beige fat cells (Fig. 2b and Supplementary Fig. 4b). This agonist-induced calcium uptake in RFP^+ beige adipocytes was further increased in the presence of Rosi, consistent with the idea that CHRNA2 forms a functional ion channel in activated beige adipocytes. (Supplementary Fig. 4g). However, no response to either agonist was detected in RFP^- white adipocytes (Fig. 2b and Supplementary Fig. 4a). We did not observe any response to acetylcholine or nicotine treatment in the RFP^+ brown fat cells that were isolated from the interscapular depot of the same mice (Fig. 2c and Supplementary Fig. 4c). This strongly suggested that the response to CHRNA2 agonists was beige fat specific. No cells from cultures of inguinal fat cells from *Chrna2* KO mice responded to agonist stimulation, suggesting that the observed response was CHRNA2 dependent (Fig. 2d and Supplementary Figs. 4d and 5a). A similar response to nicotine and acetylcholine treatment was observed via a calcium imaging assay on primary human subcutaneous fat cultures (Fig. 2e,f and Supplementary Fig. 4e), and this could be blocked by knockdown of *CHRNA2* expression in these human subcutaneous adipose cultures (Supplementary Fig. 5b), indicating that beige-like thermogenic fat cells existed in human subcutaneous depots and could be functionally regulated through CHRNA2 signaling. We further tested CHRNA2 signaling in differentiated preadipocytes isolated from human perirenal fat, a depot that has been reported to contain thermogenic adipocytes more similar to mouse classical brown fat[20–22]. Human perirenal adipocytes, although perfectly responsive to other stimuli (for example, menthol[23]), showed no response to treatment with either acetylcholine or nicotine (Fig. 2g and Supplementary Figs. 4f and 5c). Because activation of CHRNA2 was detected within the human subcutaneous fat culture but not within the perirenal fat culture, our results provide functional proof for the distinction of these two types of thermogenic fat in adult humans.

Because the calcium imaging assay indicated that the CHRNA2-containing ion channel is functional in beige adipocytes, we next investigated how CHRNA2 signaling was mediated in differentiated primary inguinal preadipocytes. The thermogenic markers *Ucp1*, *Dio2* and *Cox8b* were induced with nicotine treatment as compared to the control (Fig. 2h). It is worth noting that *Chrna2* itself was also induced after nicotine treatment (Fig. 2h). This is consistent with our previous data showing that *Chrna2* was induced during the activation of beige fat cells (Fig. 1). We observed a clear increase in levels of cAMP, a second-messenger molecule to thermogenic stimuli, and activation of protein kinase A (PKA) after nicotine stimulation of mouse inguinal fat cells (Fig. 2i). We further showed that both cAMP-responsive element binding protein (CREB) and p38 mitogen-activated kinase (p38) were activated in nicotine treated inguinal fat cells (Fig. 2i and Supplementary Fig. 6a). Similar activation of the cAMP and PKA pathway was observed in differentiated human subcutaneous adipose cultures that were stimulated with nicotine (Fig. 2j), and this activation could be blocked by treatment with the PKA inhibitor H-89 in both mouse inguinal and human subcutaneous fat cultures (Supplementary Fig. 6b). This signal was dependent on CHRNA2 with no significant compensation from other nAChR family proteins, as no activation of PKA, CREB or p38 was observed in nicotine-treated fat cells from *Chrna2* KO mice (Supplementary Fig. 6c,d). Similarly, expression of the thermogenic marker *Ucp1* was not induced by nicotine stimulation in the absence of *Chrna2* expression (Supplementary Fig. 6e).

Immune cells in subcutaneous fat produce acetylcholine. To investigate whether the activation of CHRNA2 in subcutaneous fat was mediated by locally produced acetylcholine via paracrine or autocrine mechanisms, we analyzed GFP^+ cells within the inguinal adipose tissue from $ChAT^{BAC}$-eGFP mice[24], which express enhanced green fluorescent protein (eGFP) under the control of the transcriptional regulatory element of the gene encoding choline acetyltransferase (ChAT), the rate-limiting enzyme that mediates the biosynthesis of acetylcholine in vivo (Fig. 3a). qPCR and immunohistochemistry analyses revealed that GFP^+ cells were indeed present in the inguinal adipose tissue and that they consisted of a subset of stromal vascular fraction (SVF) cells (Fig. 3b and Supplementary Fig. 7a). Enrichment of ChAT protein in inguinal SVF cells was further

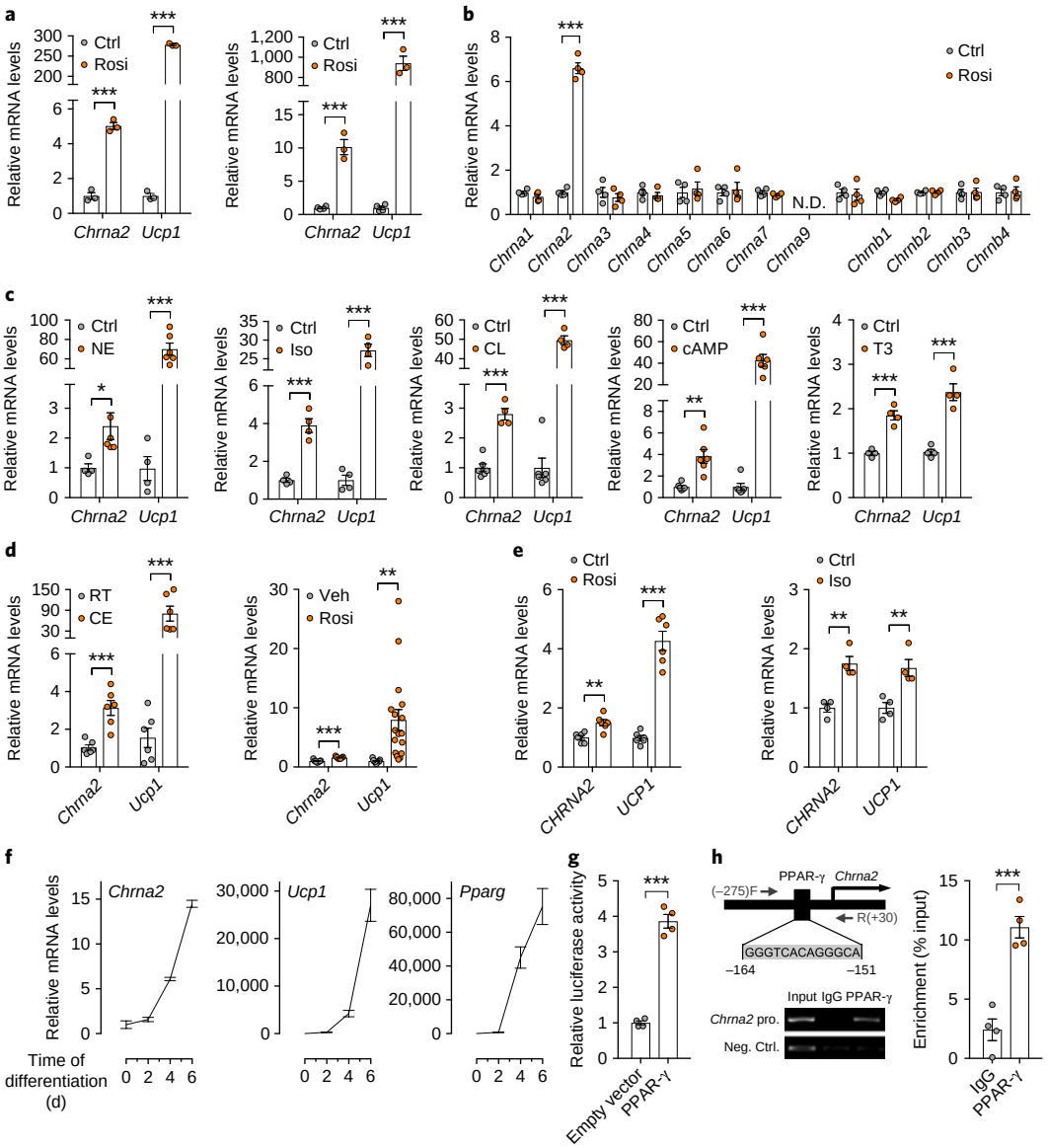

Fig. 1 | *Chrna2* is induced in subcutaneous adipocytes of mice and humans during beiging. a, Microarray (left) and qPCR (right) analyses of *Chrna2* and *Ucp1* mRNA expression in differentiated preadipocytes from WT C57BL/6J mice after treatment with vehicle control (Ctrl) or 1 μM rosiglitazone (Rosi) for 4 d (microarray, $n=3$ per group; qPCR, $n=4$ for Ctrl, $n=3$ for Rosi). **b**, qPCR analyses of mRNA levels of genes encoding nAChR subunits in differentiated inguinal preadipocytes following 1 μM Rosi treatment for 2 d, relative to that in differentiated preadipocytes treated with vehicle ($n=4$ per group). **c**, qPCR analyses of *Chrna2* and *Ucp1* mRNA expression in differentiated inguinal preadipocytes that were stimulated with vehicle (Ctrl), 0.2 μM norepinephrine (NE) for 2 d ($n=4$ for Ctrl; $n=6$ for NE), 10 μM isoproterenol (Iso) for 4 h ($n=4$ per group), 0.1 μM CL-316,243 (CL) for 24 h ($n=6$ for Ctrl; $n=4$ for CL), 500 μM dibutyryl-cAMP (cAMP) for 6 h ($n=6$ per group) or 1 μM triiodothyronine (T3) for 20 h ($n=4$ per group). **d**, qPCR analyses of *Chrna2* and *Ucp1* mRNA expression in IWAT from WT mice that were subjected to cold exposure (CE) at 4 °C or room temperature (RT) for 2 d ($n=6$ mice per group) (left) or to daily oral gavage with vehicle ($n=9$) or 20 mg per kg body weight (mg/kg) Rosi ($n=17$) for 2 weeks (right). **e**, qPCR analyses of *CHRNA2* and *UCP1* mRNA levels in differentiated human ASCs from the subcutaneous depot after exposure to vehicle, 1 μM Rosi for 4 d ($n=6$ per group) (left) or 10 μM Iso for 4 h ($n=4$ per group) (right). **f**, qPCR analyses for *Chrna2*, *Ucp1* and *Pparg* expression in the presence of 1 μM Rosi during WT inguinal preadipocyte differentiation (i.e., beige adipogenesis) ($n=3$ per group). **g**, *Chrna2* transcriptional activity analysis using a mouse *Chrna2*-promoter luciferase reporter construct with a PPAR-γ expressing vector or an empty vector as the control ($n=4$ per group). **h**, Representative gel image of ChIP analysis of PPAR-γ binding to the *Chrna2* promoter after stimulation with 1 μM Rosi for 4 d in differentiated inguinal preadipocytes (left). Graph shows enrichment relative to input ($n=4$ per group) (right). Throughout, data are presented as mean ± s.e.m. $^*P<0.05$, $^{**}P<0.01$, $^{***}P<0.001$; by two-tailed Student's *t*-test (**a**–**e**,**g**,**h**). n.d., not detected.

confirmed by flow cytometric analysis (Fig. 3c). The secretion of acetylcholine from the SVF was directly assayed and validated with mass spectrometry (Fig. 3d). We hypothesized that the local production of acetylcholine from ChAT-expressing cells within the subcutaneous fat tissue may closely correlate with the induction of its receptor, namely CHRNA2, in activated beige adipocytes. Indeed, both acetylcholine secretion and ChAT expression were higher in the SVF from cold-exposed mice as compared to those from mice that were housed at the ambient temperature (Fig. 3e). Conversely, ChAT expression in the SVF was lower in obese mice as compared that in lean mice (Supplementary Fig. 7b). To directly assess the potential role of these acetylcholine-producing SVF cells

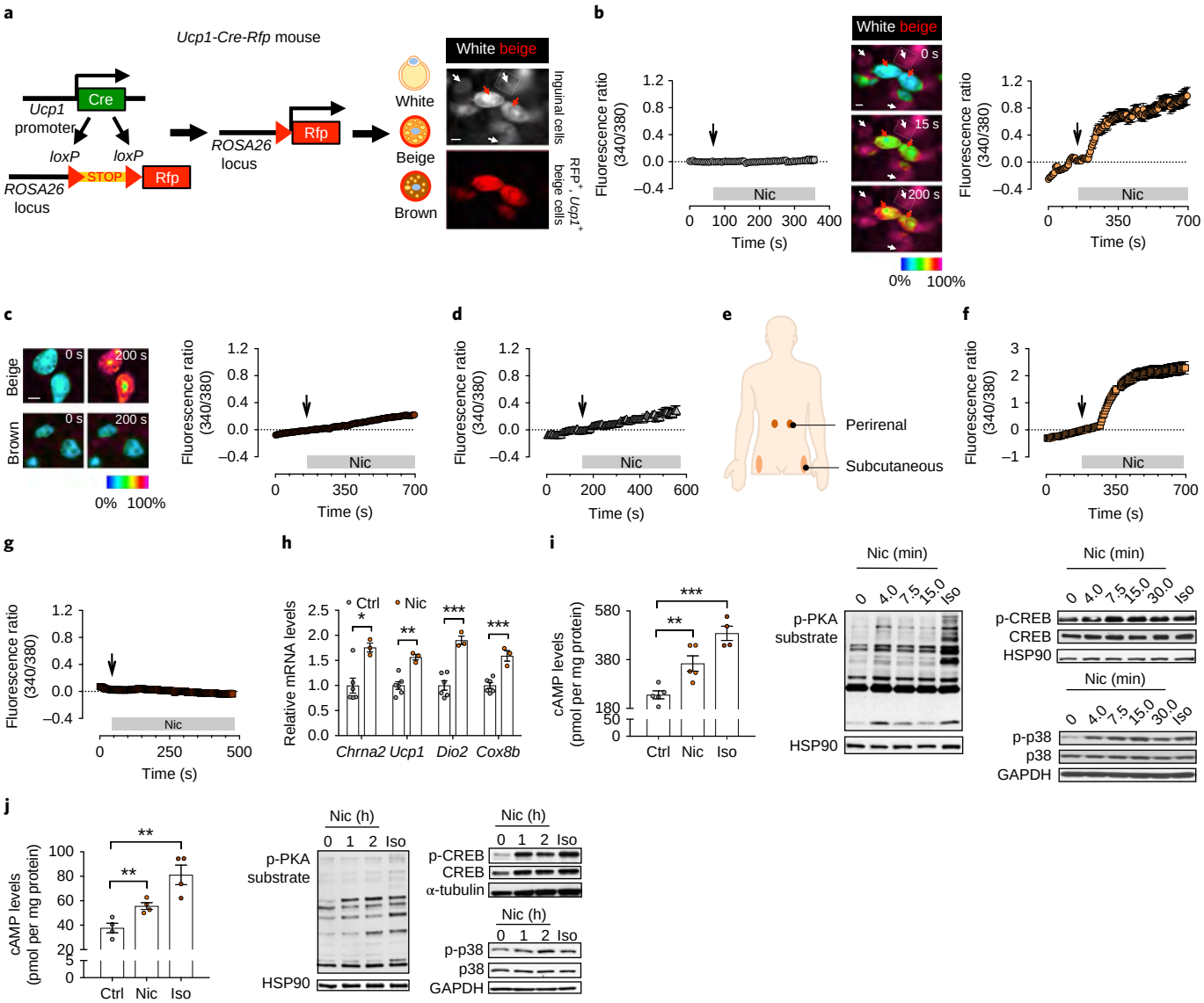

Fig. 2 | CHRNA2 signaling is beige adipocyte-selective. a, Schematic of the generation of *Ucp1-Cre-Rfp* mice. In differentiated inguinal preadipocytes, only beige adipocytes expressing RFP are visible at 550 nm (red arrows), whereas white adipocytes are not (white arrows). Scale bar, 10 μm. **b**, Intracellular Ca^{2+} rises in response to the CHRNA2 agonist nicotine (Nic, 500 μM) only in RFP^+ beige adipocytes (red arrows in images; right graph) but not in white adipocytes (white arrows in images, left graph) within the subcutaneous fat cultures. ($n=6$ for white, $n=7$ for beige). Representative images are shown in a pseudo color scale at different time points (0, 15 and 200 s). Scale bar, 10 μm. **c**, RFP^+UCP1^+ brown adipocytes of *Ucp1-Cre-Rfp* mice do not respond to Nic stimulation ($n=13$). Scale bar, 10 μm. The color bar indicates relative intracellular calcium levels from 0 (blue) to 100 (red) in **b**,**c**. **d**, Calcium uptake in response to Nic treatment is absent in the differentiated inguinal preadipocytes from *Chrna2* KO mice ($n=10$). **e**, Locations of the human subcutaneous and perirenal fat biopsy sites used in this study. **f**,**g**, Differentiated human ASCs isolated from the subcutaneous fat depot ($n=5$) (**f**), but not those from the perirenal depot ($n=11$) (**g**), mediate calcium uptake after Nic stimulation. **h**, qPCR analyses of thermogenic markers in differentiated inguinal preadipocytes of WT mice following treatment with vehicle control (Ctrl) or 2 mM Nic for 8 h ($n=6$ for Ctrl, $n=3$ for Nic). **i**, Left, cAMP levels of differentiated WT inguinal preadipocytes that were stimulated with 2 mM Nic or 10 μM isoproterenol (Iso) ($n=5$ for Ctrl and Nic, $n=4$ for Iso). Middle and right, immunoblot analysis for phosphorylation of PKA substrate (middle), and CREB and p38 (right), in differentiated inguinal preadipocytes that were exposed to 2 mM Nic for the indicated amounts of time or to 10 μM Iso for 5 min as a positive control. Heat shock protein 90 (HSP90) and glyceraldehyde 3-phosphate dehydrogenase (GAPDH) were used as loading controls. **j**, Left, cAMP levels in differentiated human ASCs from the subcutaneous depot that were treated with 2 mM Nic or 10 μM Iso ($n=4$ per group). Middle and right, immunoblots for phosphorylation of PKA substrate (middle), and CREB and p38 (right), in differentiated human ASCs after treatment with 2 mM Nic for the indicated amounts of time or with 10 μM Iso for 1 h as a positive control. HSP90, GAPDH or α-tubulin were used as loading controls. Representative images or blots are shown (Supplementary Fig. 6). Throughout, data are presented as mean ± s.e.m. (in some graphs in **b**–**g**, error bars are almost invisible). $^*P<0.05$, $^{**}P<0.01$, $^{***}P<0.001$; by two-tailed Student's *t*-test (**h**) or one-way ANOVA (**i**,**j**).

in regulating the function of neighboring adipocytes, co culture experiments were performed using a two-chamber Transwell system (Fig. 3f). The expression of thermogenic markers was elevated in differentiated inguinal fat cultures that were exposed to freshly isolated SVF as compared to that in control inguinal fat cultures (Fig. 3f), and an additional induction was detected when the coculture was performed in the presence of rivastigmine (an inhibitor of acetylcholinesterase and butyrylcholinesterase), which prevented

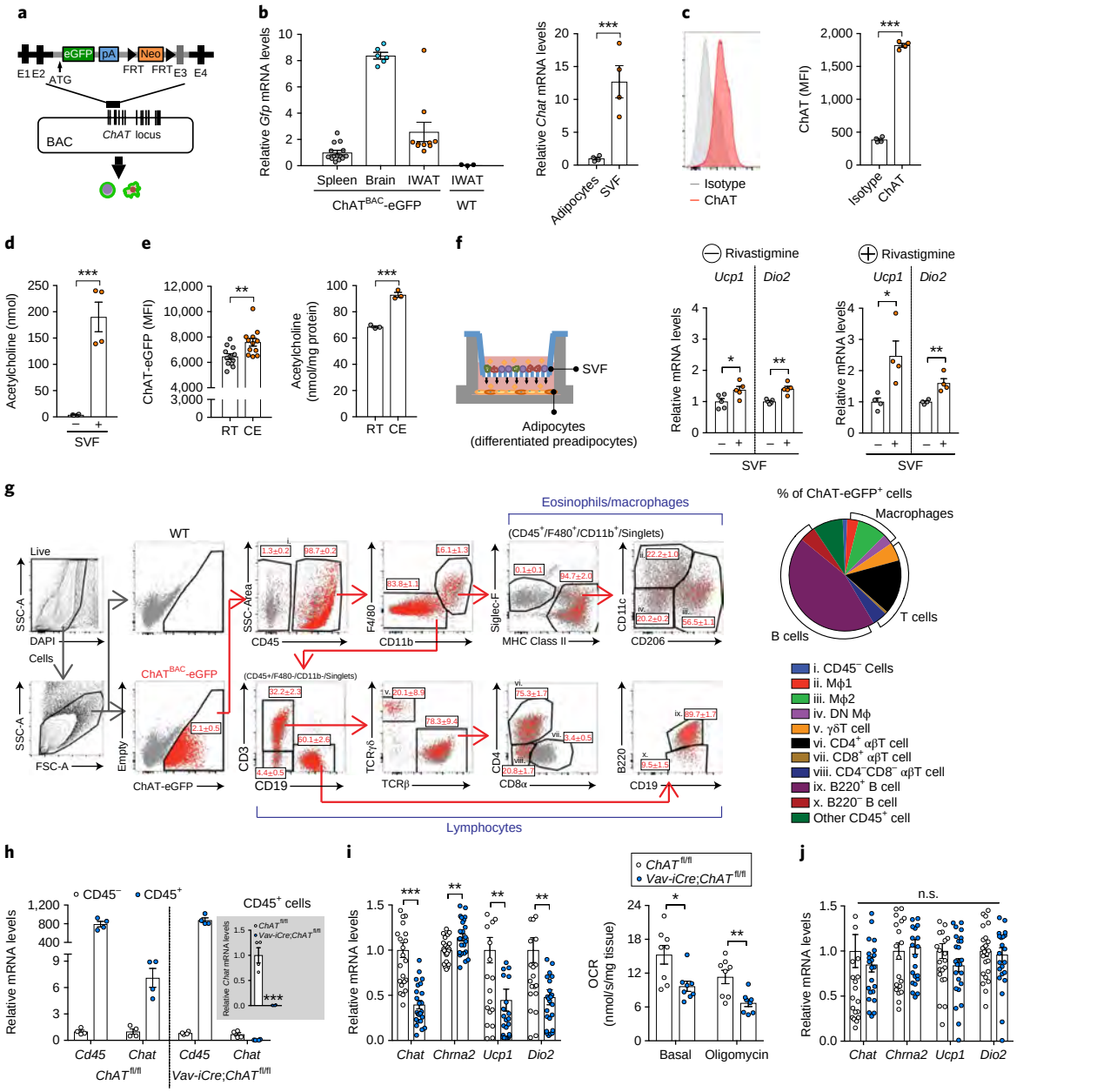

Fig. 3 | Acetylcholine-synthesizing cells of hematopoietic origin reside within inguinal subcutaneous fat tissue. a, Schematic for the generation of ChAT^{BAC}-eGFP mice. **b**, Left, qPCR analyses of *Gfp* mRNA levels in the spleen ($n=14$), the brain ($n=6$) and IWAT ($n=10$) of ChAT^{BAC}-eGFP mice and in the IWAT($n=3$) of C57BL/6 J (WT) mice (negative control). Right, qPCR analyses of *Chat* mRNA levels in the SVF and in mature adipocytes from IWAT of WT mice ($n=4$ per group). **c**, Representative histograms (left) and median fluorescence intensity (MFI) values (right) for ChAT protein expression in inguinal SVF of WT mice ($n=4$ per group). **d**, Quantification of acetylcholine levels secreted from the inguinal SVF of WT mice. PBS incubated with SVF and without SVF were labeled with "+" and "−", respectively ($n=4$ per group). **e**, Left, MFI of ChAT-eGFP in the GFP$^+$ population from inguinal SVF of ChAT^{BAC}-eGFP mice that were housed at RT or 4 °C for 4 h (CE). GFP$^+$ cells and their MFI values were monitored by flow cytometry ($n=12$ per group). Right, quantification of acetylcholine levels secreted from the inguinal SVF of WT mice that were housed at RT or CE ($n=3$ per group). **f**, Schematic showing adipocytes and SVF in a two-chamber coculture system using a bicompartmental Transwell plate (left) and qPCR analyses of thermogenic markers in differentiated WT inguinal preadipocytes that were cocultured with or without freshly isolated inguinal SVF from WT mice for 4 h in the absence ($n=5$ per group) or presence ($n=4$ per group) of rivastigmine using the two-chamber coculture system (right). **g**, Immune profiling of ChAT-expressing cells from inguinal SVF of ChAT^{BAC}-eGFP mice. Left, flow cytometric gating strategy for identifying immune cell subsets in ChAT-eGFP$^+$ cells. All immune cell subsets were labeled with numerals "i" through "x" and reported as percentages of the parent population ($n=3$ per group). Right, pie chart summarizing the relative frequencies of immune cell subsets (i–x) within the ChAT-eGFP$^+$ cell population. **h**, qPCR analyses of *Chat* mRNA levels in CD45$^-$ and CD45$^+$ cell populations collected by FACS from inguinal SVF of *Chat*$^{fl/fl}$ and *Vav-iCre*;*Chat*$^{fl/fl}$ mice ($n=4$ per group). An insert graph shows Chat mRNA levels in inguinal CD45$^+$ cells from *Vav-iCre*;*Chat*$^{fl/fl}$ mice, relative to that from *Chat*$^{fl/fl}$ mice ($n=4$ per group) **i**, Left, qPCR analyses of thermogenic markers in IWAT of *Chat*$^{fl/fl}$ and *Vav-iCre*;*Chat*$^{fl/fl}$ mice that were subjected to exposure at 4 °C for 6 h (CE) ($n=24$ per group). Right, OCR in freshly isolated inguinal fat tissue from cold-exposed *Chat*$^{fl/fl}$ and *Vav-iCre*;*Chat*$^{fl/fl}$ mice in the absence (basal) or presence of oligomycin ($n=8$ per group). **j**, qPCR analyses of thermogenic markers in the interscapular BAT from *Chat*$^{fl/fl}$ and *Vav-iCre*;*Chat*$^{fl/fl}$ mice following CE ($n=24$ per group). Throughout, data are presented as mean ± s.e.m. $^*P<0.05$, $^{**}P<0.01$, $^{***}P<0.001$. n.s., not significant; by two-tailed Student's *t*-test (**b**–**f**,**h**–**j**) or Mann–Whitney *U* test (**i**).

acetylcholine degradation (Fig. 3f), indicating that the effect was at least in part mediated through acetylcholine released from the SVF.

Flow cytometric analysis revealed that ~2.1% of the inguinal SVF of the ChAT^{BAC}-eGFP mice were GFP$^+$, showing significantly higher GFP median fluorescence intensity (MFI) and enriched expression of *Chat* compared to that in GFP$^-$ cells (Fig. 3g and Supplementary Fig. 7c). Immune profiling by flow cytometric analysis (Supplementary Table 1) revealed that the majority of ChAT-eGFP$^+$ cells were of the CD45$^+$ hematopoietic lineage (98.7 ± 0.2%). Among hematopoietic cells, B220$^+$ B cells comprised the largest proportion of immune cell subsets (44.5 ± 2.5%), followed by CD4$^+$ αβ T cells (15.6 ± 1.1%) and M2 macrophages (8.5 ± 0.4%). Of note, there were almost no ChAT-eGFP$^+$ cells that expressed the eosinophil marker Siglec-F (Fig. 3g and Supplementary Table 1). It has previously been reported that certain types of B cells or T cells can produce acetylcholine[25,26]. It is of note that ~9% of the total ChAT-eGFP$^+$ cells were characterized as alternatively activated M2 macrophages, which have been implicated to produce catecholamines that activate thermogenic fat cells[27]. The upregulation of thermogenic gene expression by coculture with SVF was detected even in the absence of β-adrenergic signaling[28], indicating that non-catecholamine stimulant(s) exerted this activating effect (Supplementary Fig. 7d). This was consistent with recent reports that have challenged the idea of secretion of catecholamine from M2 macrophages[29,30].

To investigate the physiological effect of acetylcholine-producing immune cells during beiging, we generated mice in which the *Chat* gene was deleted in CD45$^+$ hematopoietic cells (*Vav–iCre*;*Chat*$^{fl/fl}$; Fig. 3h and Supplementary Fig. 8a). We observed significantly lower *Chat* expression in inguinal white adipose tissue (IWAT) of *Vav–iCre*;*Chat*$^{fl/fl}$ mice than in that of control mice, but not in the interscapular brown adipose tissue (BAT), which is consistent with the idea that the ChAT–CHRNA2 axis is beige-selective (Supplementary Fig. 8b). The phenotype of *Vav–iCre*;*Chat*$^{fl/fl}$ mice was comparable to that of littermate *Chat*$^{fl/fl}$ controls when housed at room temperature (Supplementary Fig. 8c–g). However, hematopoietic ablation of *Chat* caused thermogenic defects in IWAT after acute cold exposure, with a significantly lower induction in thermogenic marker expression and oxygen consumption rate (OCR) as compared to those of the control mice (Fig. 3i); however, these effects were not observed in the BAT (Fig. 3j). We performed coculture experiments and observed that the induction of thermogenic markers was trending lower (although not statistically significant) in the inguinal fat cells that were cocultured with the SVF from *Vav–iCre*;*Chat*$^{fl/fl}$ mice as compared to that of littermate *Chat*$^{fl/fl}$ controls (Supplementary Fig. 8h). It is worth noting that thermogenic gene expression in IWAT was comparable after chronic cold exposure between *Vav–iCre*;*Chat*$^{fl/fl}$ mice and littermate controls (Supplementary Fig. 8i–o), suggesting that systemic acetylcholine may compensate for the loss of local acetylcholine production when a cold stimulus persists.

Loss of CHRNA2 expression affects whole-body metabolism. Our results so far demonstrate that an acetylcholine–CHRNA2 signaling axis exists within the subcutaneous adipose depot and that immune cells closely regulate beige fat activation, likely through a paracrine mechanism (Supplementary Figs. 8p and 9). Low environmental temperature greatly activates beige fat recruitment within the subcutaneous white adipose depot, so that organisms have additional thermogenic capacity to maintain core body temperature[9]. Cold exposure induced *Chrna2* expression in inguinal fat (Fig. 1d), suggesting that adaptation to cold challenges may be mediated through CHRNA2. *Chrna2* KO mice showed no gross abnormality when housed at ambient temperature (Supplementary Fig. 10a–c; see URLs). After chronic cold exposure, adipose tissues of wild-type (WT) mice underwent drastic tissue remodeling, including reduced tissue mass, which led to the reduction of overall body weight (Fig. 4a). In comparison, *Chrna2* KO mice showed significantly less body weight loss after being housed in the cold chamber (Fig. 4a). Adipose tissue mass of the visceral white fat depot (VWAT, perigonadal depot) was significantly bigger in *Chrna2* KO mice as compared to that in WT mice following cold exposure. A similar, but not statistically significant, trend was observed in the inguinal depot, whereas no mass difference was found between the two genotypes in the interscapular BAT (Fig. 4b). Histology and immunohistochemistry analyses revealed that after cold exposure, fewer UCP1$^+$ multilocular adipocytes were present in inguinal fat tissues of *Chrna2* KO mice as compared to that in WT mice, yet no differences in brown fat were observed (Supplementary Fig. 10d,e).

Gene expression analyses revealed that cold-induced activation of the thermogenic program was defective in IWAT from *Chrna2* KO mice, including the expression of thermogenic markers (*Dio2*, *Ppargc1a* and *Ucp1*), genes involved in fatty acid oxidation (*Cpt1b*, *Lcad* and *Mcad*), genes involved in lipolysis (*Atg*, *Hsl* and *Mgll*), the angiogenic gene *Vegfa* and mitochondrial genes (*Atp5b*, *Cox4*, *Cox8b*, *Cytc*, *Nd1*, *Ndufv1*, *Sdha*, *Sdhb* and *Uqcrc2*) (Fig. 4c,d). Citrate synthase is the initial enzyme of the tricarboxylic acid (TCA) cycle, and its activity often serves as a sensitive marker for mitochondrial function. Mitochondrial DNA content and citrate synthase activity were lower in the inguinal fat tissue of the cold-challenged *Chrna2* KO mice as compared to that in the inguinal tissue of the WT mice (Fig. 4e,f). Consistent with these observations, less induction of protein levels of UCP1, the mitochondrial marker COXIV and representative subunits of the respiratory complexes I–V were detected in IWAT of *Chrna2* KO mice after cold exposure as compared to that in WT mice (Fig. 4g). These led to a significantly lower level of both basal and uncoupled respiration in IWAT of *Chrna2* KO mice as compared to that in the IWAT of WT mice (Fig. 4h). Notably, the impaired adaptive thermogenic capacity caused by *Chrna2* ablation was limited to IWAT. The induction of thermogenic gene expression was not defective in the interscapular BAT from *Chrna2* KO mice after cold exposure as compared to that in WT mice (Fig. 4i). However, the defective inguinal thermogenic capacity did not cause hypothermia under the cold challenge, presumably due to a compensatory induction of skeletal muscle shivering[10,31,32] in the *Chrna2* KO mice (Supplementary Fig. 10f–j).

Because impaired energy expenditure in IWAT is closely associated with the development of obesity[33], we examined the physiological acclimation of *Chrna2* KO mice to nutrient overload. We did not observe any differences between *Chrna2* KO mice and WT mice during chow diet feeding (Supplementary Fig. 11a–g). The mutant mice showed greater weight gain on a high-fat diet (HFD) with similar food intake (Fig. 5a and Supplementary Fig. 11h). This was accompanied by higher fat content, as determined by NMR (nuclear magnetic resonance) (Fig. 5b), and larger tissue mass in all three major fat depots—IWAT, VWAT and BAT (Fig. 5c). Analysis of adipocyte size distribution showed that *Chrna2* KO mice had a lower proportion of small adipocytes but a greater proportion of large adipocytes in both IWAT and VWAT after a HFD challenge, as compared to that in WT mice (Fig. 5d,e and Supplementary Fig. 11i). Along with exacerbated weight gain, the fasting blood glucose and serum insulin levels were significantly higher in *Chrna2* KO mice than in the control mice ($P < 0.05$), indicating that insulin resistance developed in the absence of *Chrna2* signaling (Supplementary Fig. 11j,k). Consistently, the mutant mice had worsened glucose tolerance and insulin sensitivity (Fig. 5f,g). HFD feeding resulted in a lower thermogenic gene expression in the inguinal fat of *Chrna2* KO mice as compared to that in the inguinal fat of the controls, with a minimal effect in the BAT (Fig. 5h,i), and a lower whole-body energy expenditure in *Chrna2* KO mice than in the control mice (Supplementary Fig. 11l). Visceral fat of *Chrna2* KO mice that were fed a HFD had significantly higher mRNA levels of macrophage-related genes involved in inflammation and was worse in oxidative stress through NADPH oxidase activation, as compared to those

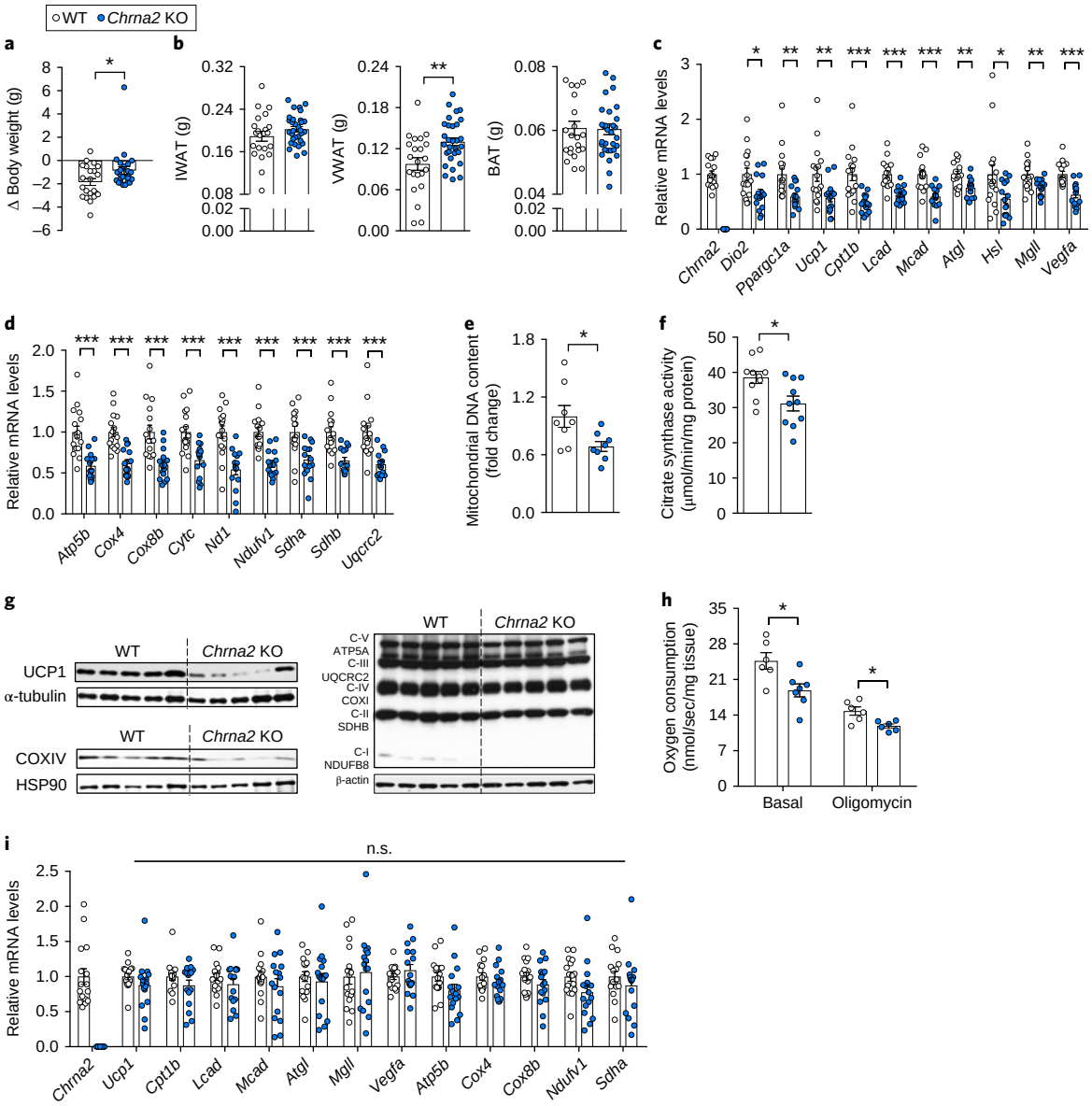

Fig. 4 | Loss of *Chrna2* reduces the adaptive thermogenic capacity of inguinal adipose tissue. a, Changes in body weight of WT and *Chrna2* KO mice following 2 weeks CE at 10 °C ($n = 22$ for WT; $n = 25$ for KO). **b**, Inguinal (IWAT), visceral (VWAT), and interscapular brown (BAT) fat mass in WT and *Chrna2* KO mice after CE ($n = 22$ for WT, $n = 31$ for KO). **c**,**d**, qPCR analyses of thermogenic genes (**c**) and mitochondrial genes (**d**) in IWAT from WT and *Chrna2* KO mice after CE ($n = 16$ for WT, $n = 15$ for KO). **e**, mitochondrial DNA content in IWAT of WT and *Chrna2* KO mice following CE ($n = 8$ per group). **f**, Citrate synthase activity in IWAT of cold-exposed WT and *Chrna2* KO mice ($n = 10$ per group). **g**, Immunoblot analyses of UCP1, the mitochondrial marker COXIV and OxPhos components in IWAT of WT and *Chrna2* KO mice after CE. Representative images from 2-3 independent experiments are shown. HSP90, α-tubulin and β-actin were used as loading controls. **h**, OCR in freshly isolated inguinal fat tissue from cold-exposed WT and *Chrna2* KO mice in the absence (basal) or presence of oligomycin ($n = 6$ for WT; $n = 7$ for KO). **i**, qPCR analyses of thermogenic markers in the interscapular BAT from WT and *Chrna2* KO mice following 2 weeks CE ($n = 16$ per group). Throughout, data are presented as mean ± s.e.m. $^*P < 0.05$, $^{**}P < 0.01$, $^{***}P < 0.001$; n.s., not significant; by two-tailed Student's *t*-test (**a**–**f**,**h**,**i**).

of control mice (Supplementary Fig. 11i). However, *Chrna2* ablation did not have a significant effect on the skeletal muscle following HFD feeding. There were no differences in locomotor activities between the two genotypes, and the effects of *Chrna2* ablation were minimal in mRNA expression of genes associated with mitochondrial oxidative phosphorylation (*Ppargc1a*, *Atp5b*, *Nd1*, *Sdha*, *Sdhb* and *Ndufv1*), which are known to be affected by HFD challenge in the skeletal muscle[34] (Supplementary Fig. 11m,n). Collectively, these results suggest that CHRNA2 signaling in beige adipocytes may provide essential protection against HFD-induced obesity and associated metabolic disorders, and that even partial loss of beige fat regulation may lead to serious detrimental consequences in systemic metabolism.

Discussion

Understanding the molecular mechanisms and signaling networks that regulate beige fat activation is of fundamental importance toward the goal of inducing it to protect against obesity in humans. We have identified a unique signaling pathway within activated beige adipocytes, which is conserved between mice and humans. The beige-selective pathway is mediated through a novel immune–adipose communication, and this previously unrecognized

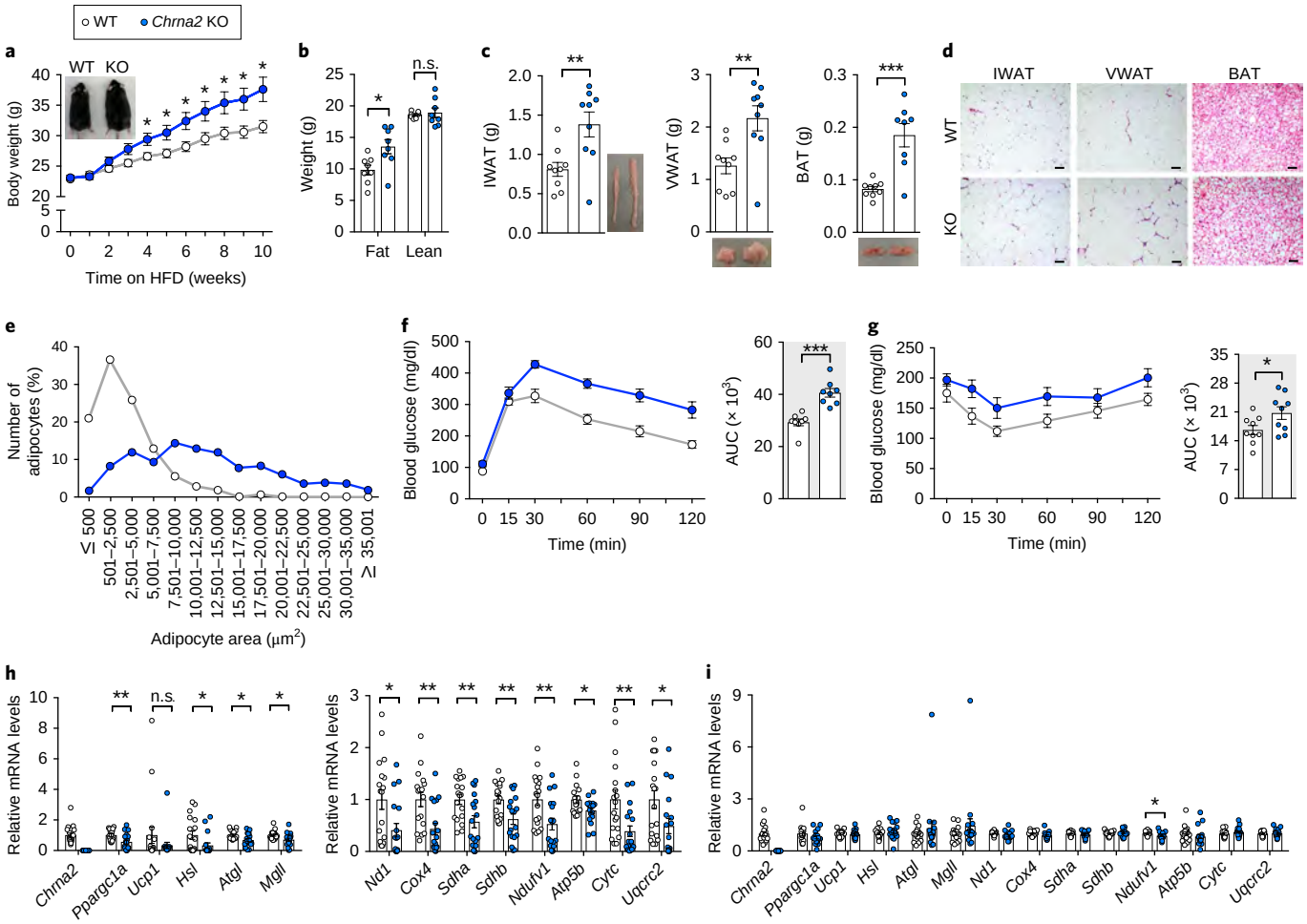

Fig. 5 | Loss of *Chrna2* exacerbates diet-induced obesity. a, Body weights of WT and *Chrna2* KO mice during high-fat diet (HFD) feeding ($n=9$ per group). **b**,**c**, Body composition ($n=8$ per group) (**b**) and fat mass ($n=9$ per group) (**c**) of WT and *Chrna2* KO mice after 10 weeks on a HFD. Images show representative fat pads from 3 independent experiments. **d**,**e**, Representative images of H&E-stained sections of IWAT, VWAT and interscapular BAT (**d**) and distribution of adipocyte size of IWAT (**e**) from WT and *Chrna2* KO mice that were fed a HFD. Scale bar, 100 μm. Representative images from 3 independent experiments in **d**. Measurements pooled from 3 mice per genotype in **e**. **f**,**g**, Intraperitoneal glucose tolerance test (GTT with 1 g/kg glucose: $n=8$ per group) (**f**) and insulin tolerance test (ITT with 0.5 U/kg insulin: $n=9$ per group) (**g**) in WT and *Chrna2* KO mice. AUC, area under the curve. **h**,**i**, qPCR analyses of thermogenic (left) and mitochondrial (right) gene expression in IWAT ($n=18$ per group) (**h**) and BAT ($n=18$ for WT; $n=19$ for KO) (**i**) of WT and *Chrna2* KO mice that were fed a HFD for 10 weeks. Throughout, data are presented as mean ± s.e.m. $^*P<0.05$, $^{**}P<0.01$, $^{***}P<0.001$; n.s., not significant; by two-tailed Student's *t*-test (**a**–**c**,**f**–**i**) or Mann–Whitney *U* test (**h**,**i**).

acetylcholine-dependent CHRNA2 signaling mechanism coordinates the integrated thermogenic response in activated beige fat. Lack of CHRNA2 signaling leads to a compromised adaptation to chronic cold challenge, dysregulates whole-body metabolism and exacerbates diet-induced obesity. It is well documented that after the onset of cold challenge, skeletal muscle and classical brown fat have an essential role in counteracting hypothermia. Indeed, snapshot evaluation of whole-body energy expenditure under cold did not reveal statistically significant differences between *Chrna2* KO mice and the controls. It is also worth pointing out that the canonical β-adrenergic regulation of beige fat remains intact within these *Chrna2* mutant mice. It has been reported that mice with deletion of beige adipocyte function are vulnerable to metabolic challenges[33]. The thermogenic defects after chronic cold exposure and metabolic dysfunction after a HFD that were observed in *Chrna2* KO mice, a model with only one branch of beige fat regulation missing, not only further confirms the physiological significance of beige adipocytes as an important metabolic regulator but also highlights the essential role of catecholamine-independent, acetylcholine–CHRNA2 signaling in energy metabolism.

It has been well reported that immune cells that reside within the adipose tissue niche closely interact with fat cells to mediate local and systemic metabolic homeostasis[35,36]. The previously uncharacterized signaling pathway described here demonstrated a dynamic interaction between the acetylcholine secreted from immune cells and the beige-fat-specific CHRNA2, and this signaling directly influenced organismal fitness after environmental challenges, such as cold and obesity. Future investigations will reveal whether one subpopulation of the ChAT-expressing immune cells within the subcutaneous fat tissue has a dominant role in the regulation of CHRNA2-conducted beige fat function. The identification of such a subset (if it exists) will help to incorporate the acetylcholine–beige fat signaling to the previously known signaling network between immune cells and adipocytes and to place this newly defined pathway within the interconnected metabolic matrix.

Nicotine, the main component of tobacco, has been implicated in the effects of smoking on body weight, presumably through central regulation on appetite[37]. It has also been observed that daily injections of nicotine for 6 months leads to decreased food intake, weight loss and induction of UCP1 in white adipose tissue in mice[38].

The activation of the thermogenic program in WAT could be, at least partially, mediated through cell-autonomous activation of CHRNA2-signaling in beige adipocytes. Meanwhile, it has been reported that changes in nerve activity influence systemic energy balance and promote WAT browning[39,40]. Therefore, it is also conceivable that chronic exposure of nicotine activates certain types of cholinergic neurons in the central and/or peripheral nervous system, increasing energy expenditure and UCP1 expression. No statistically significant differences were observed in food intake between *Chrna2* KO and control mice in our studies. Future investigations should reveal whether CHRNA2-mediated central regulation can also affect systemic metabolism.

Our discovery that nicotine activates the thermogenic program in beige adipocytes through CHRNA2 may suggest novel targets through peripheral pathways to circumvent weight gain associated with smoking cessation. Collectively, our findings suggest that the *Chrna2*-dependent pathway could present new targets for beige fat activation that can curb obesity and its related metabolic diseases in humans.

Methods

Methods, including statements of data availability and any associated accession codes and references, are available at https://doi.org/10.1038/s41591-018-0032-8.

Received: 28 February 2016; Accepted: 15 February 2018;
Published online: 21 May 2018

References

1. Wu, J. et al. Beige adipocytes are a distinct type of thermogenic fat cell in mouse and human. *Cell* **150**, 366–376 (2012).
2. Sharp, L. Z. et al. Human BAT possesses molecular signatures that resemble beige or brite cells. *PLoS One* **7**, e49452 (2012).
3. Lidell, M. E. et al. Evidence for two types of brown adipose tissue in humans. *Nat. Med.* **19**, 631–634 (2013).
4. Shinoda, K. et al. Genetic and functional characterization of clonally derived adult human brown adipocytes. *Nat. Med.* **21**, 389–394 (2015).
5. Lee, P. et al. Temperature-acclimated brown adipose tissue modulates insulin sensitivity in humans. *Diabetes* **63**, 3686–3698 (2014).
6. Hanssen, M. J. et al. Short-term cold acclimation improves insulin sensitivity in patients with type 2 diabetes mellitus. *Nat. Med.* **21**, 863–865 (2015).
7. Yoneshiro, T. et al. Recruited brown adipose tissue as an anti-obesity agent in humans. *J. Clin. Invest.* **123**, 3404–3408 (2013).
8. Chondronikola, M. et al. Brown adipose tissue improves whole-body glucose homeostasis and insulin sensitivity in humans. *Diabetes* **63**, 4089–4099 (2014).
9. Kajimura, S., Spiegelman, B. M. & Seale, P. Brown and beige fat: physiological roles beyond heat generation. *Cell Metab.* **22**, 546–559 (2015).
10. Cannon, B. & Nedergaard, J. Brown adipose tissue: function and physiological signiâcance. *Physiol. Rev.* **84**, 277–359 (2004).
11. Le Novère, N., Corringer, P. J. & Changeux, J. P. The diversity of subunit composition in nAChRs: evolutionary origins, physiologic and pharmacologic consequences. *J. Neurobiol.* **53**, 447–456 (2002).
12. Changeux, J. P. Nicotine addiction and nicotinic receptors: lessons from genetically modiâed mice. *Nat. Rev. Neurosci.* **11**, 389–401 (2010).
13. Ohno, H., Shinoda, K., Spiegelman, B. M. & Kajimura, S. PPAR-γ agonists induce a white-to-brown fat conversion through stabilization of PRDM16 protein. *Cell Metab.* **15**, 395–404 (2012).
14. Qiang, L. et al. Brown remodeling of white adipose tissue by SIRT1-dependent deacetylation of PPAR-γ. *Cell* **150**, 620–632 (2012).
15. Wilson-Fritch, L. et al. Mitochondrial remodeling in adipose tissue associated with obesity and treatment with rosiglitazone. *J. Clin. Invest.* **114**, 1281–1289 (2004).
16. Bartesaghi, S. et al. Thermogenic activity of UCP1 in human white-fat-derived beige adipocytes. *Mol. Endocrinol.* **29**, 130–139 (2015).
17. Elsen, M. et al. BMP4 and BMP7 induce the white-to-brown transition of primary human adipose stem cells. *Am. J. Physiol. Cell Physiol.* **306**, C431–C440 (2014).
18. Kong, X. et al. IRF4 is a key thermogenic transcriptional partner of PGC-1α. *Cell* **158**, 69–83 (2014).
19. Madisen, L. et al. A robust and high-throughput Cre reporting and characterization system for the whole mouse brain. *Nat. Neurosci.* **13**, 133–140 (2010).
20. Seale, P. et al. PRDM16 controls a brown fat–skeletal muscle switch. *Nature* **454**, 961–967 (2008).
21. Svensson, P. A. et al. Characterization of brown adipose tissue in the human perirenal depot. *Obesity (Silver Spring)* **22**, 1830–1837 (2014).
22. Nagano, G. et al. Activation of classical brown adipocytes in the adult human perirenal depot is highly correlated with PRDM16–EHMT1 complex expression. *PLoS One* **10**, e0122584 (2015).
23. Ma, S. et al. Activation of the cold-sensing TRPM8 channel triggers UCP1-dependent thermogenesis and prevents obesity. *J. Mol. Cell Biol.* **4**, 88–96 (2012).
24. Tallini, Y. N. et al. BAC transgenic mice express enhanced green fluorescent protein in central and peripheral cholinergic neurons. *Physiol. Genomics* **27**, 391–397 (2006).
25. Rosas-Ballina, M. et al. Acetylcholine-synthesizing T cells relay neural signals in a vagus nerve circuit. *Science* **334**, 98–101 (2011).
26. Reardon, C. et al. Lymphocyte-derived ACh regulates local innate but not adaptive immunity. *Proc. Natl. Acad. Sci. USA* **110**, 1410–1415 (2013).
27. Nguyen, K. D. et al. Alternatively activated macrophages produce catecholamines to sustain adaptive thermogenesis. *Nature* **480**, 104–108 (2011).
28. Bachman, E. S. et al. β-AR signaling required for diet-induced thermogenesis and obesity resistance. *Science* **297**, 843–845 (2002).
29. Fischer, K. et al. Alternatively activated macrophages do not synthesize catecholamines or contribute to adipose tissue adaptive thermogenesis. *Nat. Med.* **23**, 623–630 (2017).
30. Jiang, H., Ding, X., Cao, Y., Wang, H. & Zeng, W. Dense intra-adipose sympathetic arborizations are essential for cold-induced beiging of mouse white adipose tissue. *Cell Metab.* **26**, 686–692 (2017).
31. Rowland, L. A., Bal, N. C., Kozak, L. P. & Periasamy, M. Uncoupling protein 1 and sarcolipin are required to maintain optimal thermogenesis, and loss of both systems compromises survival of mice under cold stress. *J. Biol. Chem.* **290**, 12282–12289 (2015).
32. Bruton, J. D. et al. Increased fatigue resistance linked to $Ca2^{+}$-stimulated mitochondrial biogenesis in muscle åbers of cold-acclimated mice. *J. Physiol. (Lond.)* **588**, 4275–4288 (2010).
33. Cohen, P. et al. Ablation of PRDM16 and beige adipose causes metabolic dysfunction and a subcutaneous-to-visceral-fat switch. *Cell* **156**, 304–316 (2014).
34. Sparks, L. M. et al. A high-fat diet coordinately downregulates genes required for mitochondrial oxidative phosphorylation in skeletal muscle. *Diabetes* **54**, 1926–1933 (2005).
35. Brestoff, J. R. & Artis, D. Immune regulation of metabolic homeostasis in health and disease. *Cell* **161**, 146–160 (2015).
36. Lumeng, C. N. & Saltiel, A. R. Inflammatory links between obesity and metabolic disease. *J. Clin. Invest.* **121**, 2111–2117 (2011).
37. Williamson, D. F. et al. Smoking cessation and severity of weight gain in a national cohort. *N. Engl. J. Med.* **324**, 739–745 (1991).
38. Yoshida, T. et al. Nicotine induces uncoupling protein 1 in white adipose tissue of obese mice. *Int. J. Obes. Relat. Metab. Disord.* **23**, 570–575 (1999).
39. Dodd, G. T. et al. Leptin and insulin act on POMC neurons to promote the browning of white fat. *Cell* **160**, 88–104 (2015).
40. Owen, B. M. et al. FGF21 acts centrally to induce sympathetic nerve activity, energy expenditure and weight loss. *Cell Metab.* **20**, 670–677 (2014).

Acknowledgements

We thank B. M. Spiegelman and J. D. Lin for their advice and discussion throughout this work, B. Lowell (Beth Israel Deaconess Medical Center) for the β-less mice, J. M. Gimble (Tulane University) for human subcutaneous adipose precursor cells and W. Rainey (University of Michigan) for human perirenal adipose precursor cells. The work was supported by the Human Frontier Science Program (grant no. RGY0082/14; J.W.), the Edward Mallinckrodt Jr. Foundation (J.W.), the American Diabetes Association (grant no. 1-18-IBS-281; J.W.), the US National Institutes of Health (grant no. R01DK107583 (J.W.), P30-DK020572 (J.W.), P30-DK089503 (J.W.), F31DK112625 (M.P.E.), R37EB003320 (R.T.K.) and DK046960 (R.T.K.), R01-AI091627 (I.M.) and T32DA007268 (A.G.Z.)) and a postdoctoral fellowship from the American Heart Association (17POST33060001; D.K.).

Author contributions

H.J., H.Y. and J.W. designed the experiments and wrote the manuscript; H.J., H.Y., J.G., J.J., X.Q., E.P., D.K., M.P.E., A.G.Z., J.-S.C. and J.W. performed the experiments; and H.J., H.Y., J.G., E.P., A.G.Z., J.L., R.T.K., I.M., X.Z.S.X. and J.W. analyzed the data.

Competing interests

The authors declare no competing interests.

Additional information

Supplementary information is available for this paper at https://doi.org/10.1038/s41591-018-0032-8.

Reprints and permissions information is available at www.nature.com/reprints.

Correspondence and requests for materials should be addressed to J.W.

Publisher's note: Springer Nature remains neutral with regard to jurisdictional claims in published maps and institutional affiliations.

Methods

Reagents. Dexamethasone (D4902), insulin (I5500), 3-isobutyl-1-methylxanthine (IBMX, I7018), biotin (B4639), d-pantothenic acid hemicalcium salt (P5155), isoproterenol (I6504), CL-316,243 (C5976), norepinephrine (A7257), dibutyryl-cAMP (D0260), triiodothyronine (T5516), acetylcholine chloride (A2661), nicotine (N3876), (1R,2S,5R)-(−)-menthol (M2780-25G-A) and Fura 2-a.m. (F0888) were acquired from Sigma-Aldrich. Rosiglitazone (71740), GW9662 (70785), pioglitazone (71745), rivastigmine (129101-54-8) and H-89 (10010556) were obtained from Cayman Chemical. Collagenase D (11088882001), collagenase B (11088831001) and dispase II (04942078001) were purchased from Roche. Recombinant human BMP4 (314-BP-010) was acquired from R&D Systems. All of the cell culture media—including Dulbecco's modified Eagle's medium (DMEM)/F12 GlutaMAX (10565-042), DMEM (11995-073) and MesenPRO RS medium (12746-012)—and BODIPY 493/503 (4,4-difluoro-1,3,5,7,8-pentamethyl-4-bora-3a,4a-diaza-s-indacene; D3922) were purchased from Life Technologies.

Mice. All mouse studies were conducted according to the protocol that was reviewed and approved by the University Committee on Use and Care of Animals at the University of Michigan. All mice were housed under a 12-h light–12-h dark cycle (6 a.m. to 6 p.m.) with a standard rodent chow diet (5L0D - PicoLab Laboratory Rodent Diet) unless otherwise specified. The 129SVE and Balb/c mice were purchased from Taconic Farms Inc. The *Ucp1–Cre* transgenic mice, the Ai14 reporter mice, as well as the C57BL/6J, *ob/ob*, ChAT^{BAC}-eGFP, *Chat*$^{fl/fl}$, *Vav-iCre*, B6.SJL and *Chrna2*-knockout mice, were obtained from the Jackson Laboratory (stock no. 024670, 007914, 000664, 000632, 007902, 016920, 008610, 002014 and 005797, respectively). Three beta adrenergic receptors-knockout (β-less) mice were provided by Brad Lowell (Beth Israel Deaconess Medical Center, Boston). WT mice were treated with either vehicle (0.25% methylcellulose) or 20 mg per kg body weight per day rosiglitazone via oral gavage for 2 weeks. Hematopoietic-cell-specific *Chat*-deleted mice (*Vav-iCre*;*Chat*$^{fl/fl}$) were generated by crossing *Chat*$^{fl/fl}$ and *Vav-iCre* mice. Ten- to 12-week-old *Chrna2* KO mice and either WT C57BL/6J or littermate WT controls were used in cold-exposure and HFD studies. Similar results were obtained with either control group. For cold-exposure studies, mice were singly housed in pre-chilled cages in an environmental chamber kept at 10 °C for 2 weeks, unless otherwise specified. Age-matched WT and *Chrna2* KO mice were single-housed and maintained on either a chow diet or a HFD that consisted of 45% of calories from fat (D12451, Research Diets) for 10 weeks to perform the HFD-induced obesity study. Body weight and food intake were measured weekly for 10 weeks. Food intake was determined by subtracting the weight of remaining food from that of the provided food for singly housed mice.

Primary cell culture. The isolation, culture and differentiation of primary SVF from adipose depots were performed as described previously[1]. Briefly, fat tissues were dissected, minced and digested in a solution of collagenase (1.5 U/ml) (collagenase D for inguinal fat, and collagenase B for interscapular brown fat) and dispase II (2.4 U/ml), which was supplemented with 10 mM $CaCl_2$, for 15–20 min in a 37 °C water bath with agitation. Digested tissues were filtered through a 100-μm cell strainer, and the filtrate was centrifuged at 300*g*–500 *g* for 5 min to pellet cells. The floating mature adipocytes were collected when they were needed for gene expression analyses. The cell pellet was resuspended and passed through a 40-μm cell strainer, and the filtrate was centrifuged as described above. The cell pellet was resuspended with culture medium (DMEM/F12 GlutaMAX containing 15% FBS and penicillin–streptomycin) and plated onto a collagen-coated 10-cm cell culture dish. For adipocyte differentiation, confluent cultures of cells were exposed to induction medium (DMEM/F-12 GlutaMAX supplemented with 10% FBS, penicillin–streptomycin, 0.5 μg/ml insulin, 5 μM dexamethasone, 1 μM rosiglitazone and 0.5 mM IBMX). Two days after induction, cells were cultured in maintenance medium (DMEM/F-12 GlutaMAX containing 10% FBS, penicillin–streptomycin and 0.5 μg/ml insulin) until they were ready for analyses.

Human adipose precursor cells from the subcutaneous adipose tissue were acquired from liposuction that was performed on healthy adults (a gift from Jeffrey M. Gimble at Tulane University, New Orleans, Louisiana, USA), and human perirenal adipose precursor cells were isolated from donors postmortem (a gift from William Rainey at the University of Michigan, Ann Arbor, Michigan, USA). All specimens were collected under the protocols reviewed and approved by the Western Institutional Review Board (Puyallup, WA) or the University of Michigan Medical School Institutional Review Board (IRBMED). Cells were cultured in MesenPRO RS medium supplemented with penicillin–streptomycin and stimulated to differentiate in DMEM/F12 GlutaMAX, supplemented with 10% FBS, 5 μM dexamethasone, 0.5 μg/ml insulin, 0.5 mM IBMX, 5 μM rosiglitazone, 33 μM biotin, 17 μM pantothenic acid and 20 ng/ml BMP4, for 3 d. On the fourth day, cells were cultured in maintenance medium (DMEM/F12 GlutaMAX containing 10% FBS, 0.5 μg/ml insulin, 5 μM dexamethasone, 33 μM biotin and 17 μM pantothenic acid) until they were fully differentiated.

Transcriptional profiling. Total RNA was isolated from differentiated inguinal SVF that were treated with rosiglitazone (1 μM for 4 d) or a vehicle control and used for microarray analysis. Array hybridization and scanning were performed by the Dana-Farber Cancer Institute Core Facility using Affymetrix Gene Chip Mouse Genome 430 2.0 arrays, according to established methods.

Gene expression analysis. Total RNA from adipose tissue and cultured cells were extracted using the TRIzol method. For quantitative real-time PCR (qPCR) analysis, an equal amount of RNA was used to synthesize cDNA according to the instruction for M-MLV Reverse Transcriptase (Life Technologies). qPCR reactions were performed in a 384-well format using SYBR Green (Thermo Fisher Scientific). Relative mRNA levels were calculated using the $\Delta\Delta C_T$ method and normalized to levels of TATA-box binding protein (*Tbp*). The primer sequence information is shown in Supplementary Table 2.

Luciferase reporter assay. To construct the luciferase reporter with the promoter of the mouse *Chrna2* gene, the −1,053 to +31 region of mouse *Chrna2* gene was amplified by PCR using mouse genomic DNA. The amplified fragment was digested with *MluI* and *XhoI*, and the resulting fragment was cloned into the pGL3 basic vector (Promega) upstream of the firefly-luciferase-encoding region. HEK293 cells (ATCC, CRL-1573) were plated onto a 12-well plate and transiently transfected using the polyethylenimine (Thermo Fisher Scientific) method with 909 ng of a PPAR-γ-expressing, 90.9 ng of the reporter and 10 ng of *Renilla*-luciferase-expressing (internal control) plasmids. Cells were cultured for 48 h before harvest. Luciferase activity was measured by the Dual-Luciferase Assay kit (Promega) according to the manufacturer's recommendations, using a SpectraMax L (Molecular Devices) plate reader. Firefly luciferase activity was normalized to *Renilla* luciferase activity.

Chromatin immunoprecipitation (ChIP) assay. Differentiated primary inguinal preadipocytes were cross-linked with 1% formaldehyde at room temperature for 7 min and lysed with ChIP cell lysis buffer (10 mM Tris-HCl, pH 8.0, 10 mM NaCl, 3 mM $MgCl_2$, 0.5% NP-40 and protease inhibitor cocktail) and ChIP nuclear lysis buffer (50 mM Tris-HCl, pH 8.0, 5 mM EDTA, 1% SDS and protease inhibitor cocktail). The cell lysates were sonicated to shear the chromatin and immunoprecipitated with antibodies specific for PPAR-γ (#sc-7196, Santa Cruz) or IgG (#2729, Cell Signaling). The immunoprecipitants were isolated using protein A–agarose beads (Invitrogen), and these were washed and eluted with 1% SDS in 0.1 M $NaHCO_3$. After reversing the cross-links by incubation at 65 °C overnight and proteinase K digestion, the immunoprecipitated DNA fragments and input DNA were recovered by a PCR purification kit (Qiagen). The purified DNA was used to amplify the PPAR-γ regulatory element on the mouse *Chrna2* promoter by a PCR reaction. The PCR products were visualized by electrophoresis on an agarose gel containing ethidium bromide under ultraviolet (UV) light and quantified using ImageJ software. Primers directed at 7 kb upstream of the binding site were used as a negative control.

BODIPY (493/503) staining. To stain lipid droplets, differentiated inguinal preadipocytes of *Ucp1–Cre–Rfp* mice were fixed in 10% formalin, washed with PBS and incubated in PBS supplemented with 0.01 mg/ml of the fluorescent neutral lipid dye, BODIPY 493/503, at 4 °C for 30 min in the dark. The cells were washed with PBS and imaged with a fluorescent inverted Leica DMIRB microscope.

Calcium imaging. SVF isolated from mouse inguinal, mouse interscapular brown, human subcutaneous and human perirenal depots were seeded on collagen-coated glass-bottom culture dishes (MatTek Corporation) and induced to differentiate. Fully differentiated adipocytes were loaded with 10 μM of Fura 2-a.m. for 30 min at 37 °C. After 30 min they were washed twice with standard Tyrode's solution (135 mM NaCl, 4 mM KCl, 10 mM glucose, 10 mM HEPES, 2 mM $CaCl_2$ and 1 mM $MgCl_2$, pH 7.4) at room temperature. Calcium imaging was performed on an Olympus BX51WI Axiovert microscope under a 40× objective lens. Fluorescence images were documented after sequential excitation with 340-nm-wavelength light followed by 380-nm-wavelength light with a Roper CoolSnap charge-coupled device (CCD) camera. After establishing a baseline 340 nm/380 nm ratio, the CHRNA2 agonist (500 μM nicotine or 100 μM acetylcholine) was perfused onto the cells. Images were processed with MetaFlour software (Olympus). At 0 s, the basal pseudo color of beige adipocytes and white adipocytes were different, (blue versus pink), reflecting that the color in beige fat cells was the combination of the calcium-sensing fluorescent dye Fura 2-a.m. and RFP, whereas white fat cells only had the Fura 2-a.m. dye.

Short hairpin RNA (shRNA)-mediated knockdown of gene expression. Adenovirus-delivered shRNA targeting human *CHRNA2* was generated by cloning a designed shRNA into the pAdTrack-H1 vector and constructing the adenovirus using the AdEasy system, as described previously[41]. To make the adenoviral construct encoding the *CHRNA2*-specific shRNA (shCHRNA2), the primers used were as follows: forward, 5′-GATCCCCCGTTCCTAG CTGGAATGATCTTTCAAGAGAAGATCATTCCAGCTAGGAACGTT TTTA-3′; reverse, 5′-AGCTTAAAAACGTTCCTAGCTGGAATGATCT TCTCTTGAAAGATCATTCCAGCTAGGAACGGGG-3′. The generated adenovirus expressing shCHRNA2 also expressed GFP, which allowed us to verify and visually monitor the infection. To knockdown *CHRNA2* expression in human

subcutaneous adipocytes, differentiated human adipose precursor cells were transduced with adenovirus expressing shCHRNA2 and further cultured for 3 d. An adenovirus encoding GFP was used as a control.

Cellular cAMP levels. cAMP was extracted with 0.1 M HCl from differentiated primary preadipocytes and then quantified using a competitive enzyme immunoassay kit according to manufacturer's instructions (Cayman Chemical).

Immunoblotting. Total protein from fat tissues and differentiated primary preadipocytes was prepared in ice-cold lysis buffer (50 mM Tris-HCl, pH 7.5, 1% Triton X-100, 1% sodium deoxycholate, 0.1% SDS, 150 mM NaCl and 1 mM phenylmethylsulfonyl fluoride) supplemented with a protease inhibitor cocktail (Roche) and phosphatase inhibitors (10 mM NaF, 60 mM β-glycerolphosphate, pH 7.5, 2 mM sodium orthovanadate and 10 mM sodium pyrophosphate). Proteins were subjected to SDS–PAGE and transferred onto polyvinylidene difluoride (PVDF) membranes. The membranes were probed with antibodies to the following proteins: UCP1 (ab10983; Abcam; 1:10,000), MitoProfile total OXPHOS (ab110413; Abcam; 1:250), COXIV (#4850; Cell Signaling; 1:4,000), phospho-PKA substrate$^{S/T}$ (#9621; Cell Signaling; 1:2,000), phospho-CREB^{S133} (#9198; Cell Signaling; 1:3,000), CREB (#9212; Cell Signaling; 1:3,000), phospho-p38^{T180,Y182} (#9215; Cell Signaling; 1:3,000), p38 (#9197; Cell Signaling; 1:3,000) α-tubulin (#2144; Cell Signaling; 1:5,000), β-actin (#8457; Cell Signaling; 1:5,000), GAPDH (#5174; Cell Signaling; 1:5,000) and HSP90 (#4874; Cell Signaling; 1:3,000). Levels of phosphorylated CREB and p38 were normalized to total CREB and p38, respectively, and were quantified using ImageJ software.

Immunofluorescence staining. Inguinal fat and brain tissues were fixed in formalin (10%) after dissection. After washing with PBS, tissues were dehydrated in 15% sucrose for 2 d and in 30% sucrose for another 3 d. Following embedding in OCT (Sakura), tissues were sectioned at 16–20 µm. The sections were blocked in 2% normal donkey serum, 3% BSA and 0.2% Triton X-100 in PBS for 1 h and incubated with a rabbit polyclonal antibody specific for GFP (A-6455, Life Technologies) at a 1:400 dilution overnight. Following incubation with an Alexa-Fluor-488-conjugated secondary antibody (ab150073, Abcam; 1:1,000) for 1 h at room temperature, slides were mounted with ProLong Gold antifade reagent with DAPI (P36935, Thermo Fisher Scientific) and imaged with a LEICA DM2000.

Acetylcholine (Ach) quantification. Inguinal SVF was isolated from C57BL/6 J mice, as described above in primary cell culture section, and washed with PBS. The SVF was incubated in PBS supplemented with 150 µM rivastigmine for 40 min at room temperature and then centrifuged to collect the supernatant, which contained the Ach produced from the SVF. Ach was measured using a previously described liquid chromatography coupled to tandem mass spectrometry (LC-MS/MS) assay for neurotransmitters[42]. Briefly, d4-Ach (C/D/N isotopes, Pointe-Claire, Canada) was added to samples as an internal standard, and the resulting samples were separated by liquid chromatography using the Thermo Scientific TSQ Quantum LCMS system. Mobile phase A was 10 mM ammonium formate and 0.15% (vol/vol) formic acid in water. Mobile phase B was acetonitrile. The gradient was: initial, 5% B; 0.1 min, 19% B; 1 min, 26% B; 1.5 min, 75% B; 2.50 min, 100% B; 3.0 min, 100% B; 3.1 min, 5% B; 3.5 min, 5% B; 4.0 min, 0% B. Ach and d4-Ach were measured by MS/MS using the following transitions (*m/z*): Ach (product: 146, precursor: 87) and d4-Ach (product: 150, precursor: 91). Quantification was done by using the ratio of the peak areas of Ach that were divided by the area of the internal standard for Ach (d4-Ach) in comparison to the calibration curves.

Adipocyte and SVF coculture assay. Adipocytes and SVF were cocultured in a bicompartmental system using Corning Transwell plates (Corning). Isolated inguinal SVF was seeded and differentiated in the lower compartment of the Transwell plates, as described above. When adipocytes in the lower compartment were fully differentiated, freshly harvested inguinal SVF was introduced in the upper compartment. The cells were cocultured in DMEM/F12 containing 10% FBS, 1% penicillin–streptomycin and 0.5 µg/ml insulin, with a polycarbonate membrane (0.4-µm pores) between the two compartments, for 4 h at 37 °C in 5% CO_2. The adipocytes were then collected from the lower compartment to analyze gene expression by qPCR.

Flow cytometric analysis. Isolated SVF from inguinal tissues was blocked in a mixture of normal rat and mouse serum on ice for 15 min and incubated with antibodies to the following proteins for immune profiling: CD45 (30-F11, BioLegend), F4/80 (BM8, BioLegend), CD11b (M1/70, Biolegend), MHC class II (M5/114.15.2, BioLegend), Siglec-F (E50-2440, BD Biosciences), CD11c (N418, BioLegend), CD206 (MR5D3, BioLegend), CD3 (17A2, BioLegend; 17A2, BioLegend), TCR-γδ (UC7-13D5, BioLegend), TCR-β (H57-597, BioLegend), CD4 (GK1.5, BioLegend), CD8 (53-6.7, BioLegend), CD19 (1D3/CD19, BioLegend) and B220 (Ra3-6B2, BioLegend). Dead cells were initially excluded based on DAPI (4,6-diamidino-2-phenylindole) uptake, and then debris were eliminated using side scatter area (SSC-A) versus forward scatter area (FSC-A). Inguinal SVF of WT mice served as a negative control to identify the ChAT-eGFP$^+$ cell population. The ChAT-eGFP$^+$ cells were gated on hematopoietic lineage (CD45) and subsequently on myeloid cells (F4/80 and CD11b). Singlets were separately selected from ChAT-eGFP$^+$ myeloid cells (CD45$^+$F4/80$^+$CD11b$^+$) and ChAT-eGFP$^+$ non-myeloid cells (CD45$^+$F4/80$^-$CD11b$^-$) using SSC-A versus SSC-width (not shown) to identify eosinophil–macrophage subsets (Siglec-F, eosinophil; MHC class II, pan-macrophages; CD11c, M1 macrophages; CD206, M2 macrophages) and lymphocyte subsets (CD3, TCR-γδ, TCR-β, CD4 and CD8-α for T cells; CD19 and B220 for B cells), respectively. For intracellular analysis of ChAT expression, the SVF was fixed and permeabilized using BD Cytofix/Cytoperm kit (BD Biosciences) and then incubated with a rabbit monoclonal ChAT antibody (ab181023, Abcam) or isotype IgG control followed by BV421-conjugated anti-rabbit secondary antibody (BioLegend). Dead cells were excluded using the Zombie Aqua Fixable Viability Kit (BioLegend). Flow cytometry acquisition was performed on a three-laser Fortessa flow cytometer (Becton Dickinson), and data were analyzed with FlowJo software (TreeStar).

Bone marrow transplantation (BMT). Bone marrow cells (1×10^6) from adult *Chrna2* KO and littermate WT control mice (CD45.2) were transplanted into lethally irradiated (2×550 cGy, 4 h apart) recipient B6.SJL mice (CD45.1). After 6 weeks (to allow for full reconstitution by the transplanted bone marrow), we confirmed that myeloid and B cells showed a complete turnover in both WT and *Chrna2* KO BMT recipient mice[43].

Histology. Adipose tissues were dissected and fixed in 10% formalin overnight at 4 °C. Paraffin-embedding and hematoxylin and eosin (H&E) staining were performed by the University of Michigan Comprehensive Cancer Center Research Histology and Immunoperoxidase Laboratory. Adipocyte size was analyzed with H&E-stained images of sections of WT and *Chrna2* KO IWAT and VWAT (three mice per genotype), using ImageJ software (Adiposoft[44]).

Respiration. Freshly isolated inguinal tissues were weighed and minced in respiration buffer (2.5 mM glucose, 50 µM palmitoryl-l -carnitine hydrochloride, 2.5 mM malate, 120 mM NaCl, 4.5 mM KCl, 0.7 mM Na_2HPO_4, 1.5 mM NaH_2PO_4 and 0.5 mM $MgCl_2$, pH 7.4). Tissue oxygen consumption in the respiration buffer was recorded for 1–2 min at each stage (basal or uncoupled) using a Clark electrode (Strathkelvin Instruments). 4 mg/ml oligomycin (Sigma) was acutely added to the respiration chamber to measure the uncoupled respiration.

Mitochondrial DNA copy-number analysis. Total DNA was isolated from mouse inguinal fat tissue using Tri-reagent (Sigma) according to the manufacturer's instructions. To estimate mitochondrial DNA copy number, the relative amounts of nuclear and mitochondrial DNA were determined by qPCR with primers specific to the *CoxI* region of the mitochondrial genome and to *Rip140*, as a nuclear marker gene.

Citrate synthase activity. Inguinal tissues were homogenized in extraction buffer (50 mM Tris-HCl, 1 mM $MgCl_2$, 100 mM KCl, 250 mM sucrose and 30 mM 2-mercaptoethanol) and centrifuged at 1,000 *g* for 15 min at 4 °C. Citrate synthase activity in the supernatant was measured with a citrate synthase activity assay kit according to manufacturer's instructions (Cayman Chemical).

Immunohistochemistry. Excised inguinal and brown adipose tissues were fixed in 10% formalin for 24 h and then were embedded in paraffin and sectioned at 5 µm by the University of Michigan Comprehensive Cancer Center Research Histology and Immunoperoxidase Laboratory. Sections were deparaffinized in xylene, rehydrated in ethanol and distilled water, and then microwaved in 10 mM sodium citrate buffer (pH 6.0) for antigen retrieval. Endogenous peroxidase was quenched with hydrogen peroxide in methanol for 30 min. Sections were blocked with 3% BSA for 1 h and incubated with rabbit polyclonal anti-UCP1 antibody (1:200; ab10983, Abcam) in 3% BSA overnight at 4 °C. PBS-washed sections were incubated with biotinylated anti-rabbit antibody for 1 h and exposed to 3,3′ -diaminobenzidine (DAB, Vector Laboratories) for 2 min to develop the signal. Hematoxylin was used to counterstain sections. The images were visualized and captured randomly from the stained sections using a LEICA DM2000 microscope.

Metabolic phenotyping. Blood glucose and serum insulin levels of 4-h-fasted mice were measured using the OneTouch Ultra Glucometer (Lifescan) and an insulin ELISA kit (Crystal Chem Inc), respectively. For the glucose tolerance test (GTT), overnight-fasted mice were injected intraperitoneally with 1 g/kg glucose. For the insulin tolerance test (ITT), mice were fasted for 4 h and then received an intraperitoneal injection of 0.5 U/kg insulin (Humulin R, Eli Lilly). GTT and ITT were done 9 and 8 weeks after HFD feeding, respectively. Glucose levels were measured in tail blood before and at the indicated times following the injection. The area under the curve (AUC) was calculated for the GTT and ITT with Prism 6 (GraphPad Software, Inc.). University of Michigan Animal Phenotyping Core determined the body composition (quantification of fat and lean mass) using nuclear magnetic resonance (NMR) analysis. Oxygen consumption (VO_2), carbon dioxide production (VCO_2) and spontaneous locomotor activity (at the *x* axis and *y* axis) were monitored for 48 h using a Comprehensive Laboratory Monitoring System (Columbus Instruments) equipped with photo beam sensors

at the University of Michigan Animal Phenotyping Core. Energy expenditure was estimated with VO_2 and VCO_2 (ref.[45]). Body temperature was monitored using a RET-3 mouse rectal probe (World Precision Instruments).

Statistical analyses. All results are presented as mean ± s.e.m. and were graphed using Prism 6. Data are representative of 2–4 independent experiments. Sample sizes were biological replicates and were chosen based on preliminary data or previously published reports. We first performed normality tests using the Shapiro–Wilk test ($3 \leq n \leq 7$) or the D'Agostino–Pearson omnibus test ($n \geq 8$). Normally distributed data were further analyzed by parametric tests including a two-tailed Student's *t*-test for two-group comparisons or a one-way analysis of variance (ANOVA) for multiple comparisons involving one independent variable. When groups followed a non-normal distribution, the Mann–Whitney *U* test was used. Data for whole-body energy expenditure in the HFD study were analyzed by using analysis of covariance (ANCOVA) with body weight as a covariate, as body weight was significantly different between WT and *Chrna2* KO mice that were fed a HFD. $P < 0.05$ was considered to be statistically significant, and P values were noted as $^{*}P < 0.05$, $^{**}P < 0.01$ and $^{***}P < 0.001$.

Reporting Summary. Further information on experimental design is available in the Nature Research Reporting Summary linked to this article.

Data availability. Accession code for the deposited microarray is GSE79031. The dataset generated in the current study is available from the corresponding author on reasonable request. Uncropped immunoblot images available in Supplementary Fig. 12.

URLS. Phenotypic analysis of Chrna2 *Chrna2* KO mice; http://www.informatics.jax.org/knockout_mice/deltagen/1658.html.

References

41. Luo, J. et al. A protocol for rapid generation of recombinant adenoviruses using the AdEasy system. *Nat. Protoc.* **2**, 1236–1247 (2007).
42. Song, P., Mabrouk, O. S., Hershey, N. D. & Kennedy, R. T. In vivo neurochemical monitoring using benzoyl chloride derivatization and liquid chromatography–mass spectrometry. *Anal. Chem.* **84**, 412–419 (2012).
43. Goldschneider, I., Komschlies, K. L. & Greiner, D. L. Studies of thymocytopoiesis in rats and mice. I. Kinetics of appearance of thymocytes using a direct intrathymic adoptive transfer assay for thymocyte precursors. *J. Exp. Med.* **163**, 1–17 (1986).
44. Galarraga, M. et al. Adiposoft: automated software for the analysis of white adipose tissue cellularity in histological sections. *J. Lipid Res.* **53**, 2791–2796 (2012).
45. Weir, J. B. New methods for calculating metabolic rate with special reference to protein metabolism. 1949. *Nutrition* **6**, 213–221 (1990).

nature research

Corresponding author(s): Jun Wu

Life Sciences Reporting Summary

Nature Research wishes to improve the reproducibility of the work that we publish. This form is intended for publication with all accepted life science papers and provides structure for consistency and transparency in reporting. Every life science submission will use this form; some list items might not apply to an individual manuscript, but all fields must be completed for clarity.

For further information on the points included in this form, see Reporting Life Sciences Research. For further information on Nature Research policies, including our data availability policy, see Authors & Referees and the Editorial Policy Checklist.

Please do not complete any field with "not applicable" or n/a. Refer to the help text for what text to use if an item is not relevant to your study.
For final submission: please carefully check your responses for accuracy; you will not be able to make changes later.

Experimental design

1. Sample size

   Describe how sample size was determined.

   Sample sizes are biological replicates and were chosen based on preliminary data or previously published reports. We first performed normality tests using the Shapiro-Wilk test ($3 \le n \le 7$) or the D'Agostino–Pearson omnibus test ($n \ge 8$). Normally distributed data were further analyzed by parametric tests including a two-tailed Student's t-test for two-group comparisons or a one-way analysis of variance (ANOVA) for multiple comparisons involving one independent variable. When groups followed a non-normal distribution, Mann–Whitney U test was used.

2. Data exclusions

   Describe any data exclusions.

   No data were excluded from the analyses

3. Replication

   Describe the measures taken to verify the reproducibility of the experimental findings.

   Data are representative of 2-4 independent experiments.

4. Randomization

   Describe how samples/organisms/participants were allocated into experimental groups.

   For all animal experiments, the animals were randomly assigned at the time of purchase or weaning to minimize any possible bias. Age-matched mice were used for in vivo studies.

5. Blinding

   Describe whether the investigators were blinded to group allocation during data collection and/or analysis.

   Histology was performed blinded. CLAMS were performed by a staff scientist at the University of Michigan Animal Phenotyping Core without in-depth knowledge about the scope of the current work. Other experiments were not blinded.

Note: all in vivo studies must report how sample size was determined and whether blinding and randomization were used.

6. Statistical parameters

For all figures and tables that use statistical methods, confirm that the following items are present in relevant figure legends (or in the Methods section if additional space is needed).

n/a	Confirmed
☐	☒ The exact sample size (*n*) for each experimental group/condition, given as a discrete number and unit of measurement (animals, litters, cultures, etc.)
☐	☒ A description of how samples were collected, noting whether measurements were taken from distinct samples or whether the same sample was measured repeatedly
☐	☒ A statement indicating how many times each experiment was replicated
☐	☒ The statistical test(s) used and whether they are one- or two-sided *Only common tests should be described solely by name; describe more complex techniques in the Methods section.*
☐	☒ A description of any assumptions or corrections, such as an adjustment for multiple comparisons
☐	☒ Test values indicating whether an effect is present *Provide confidence intervals or give results of significance tests (e.g. P values) as exact values whenever appropriate and with effect sizes noted.*
☐	☒ A clear description of statistics including central tendency (e.g. median, mean) and variation (e.g. standard deviation, interquartile range)
☐	☒ Clearly defined error bars in all relevant figure captions (with explicit mention of central tendency and variation)

See the web collection on statistics for biologists for further resources and guidance.

Software

Policy information about availability of computer code

7. Software

Describe the software used to analyze the data in this study.

All results are presented as mean ± s.e.m. and graphed using Prism 6. Images in Calcium Imaging experiments were processed with MetaFlour software (Olympus). Flow cytometry acquisition was performed on a 3-laser Fortessa flow cytometer (Becton Dickinson) and data were analyzed with FlowJo software (TreeStar). Image quantification for western blot was performed using ImageJ software. Adipocyte size was analyzed using ImageJ software (Adiposoft).

For manuscripts utilizing custom algorithms or software that are central to the paper but not yet described in the published literature, software must be made available to editors and reviewers upon request. We strongly encourage code deposition in a community repository (e.g. GitHub). *Nature Methods* guidance for providing algorithms and software for publication provides further information on this topic.

Materials and reagents

Policy information about availability of materials

8. Materials availability

Indicate whether there are restrictions on availability of unique materials or if these materials are only available for distribution by a third party.

All the materials, cells, and animals used in the paper are available upon request under MTA with the University of Michigan.

9. Antibodies

Describe the antibodies used and how they were validated for use in the system under study (i.e. assay and species).

ChIP assay was performed with antibodies for PPARγ (#sc-7196, Santa Cruz) or IgG (#2729, Cell Signaling). Western blot was performed with following antibodies: from Abcam: UCP1 (ab10983), MitoProfile total OXPHOS (ab110413); from Cell Signaling: COXIV (#4850), phospho-PKA substrateS/T (#9621), phospho-CREBS133 (#9198), CREB (#9212), phospho-p38T180/Y182 (#9215), p38 (#9197) α-tubulin (#2144), β-actin (#8457), GAPDH (#5174), and HSP90 (#4874). Immunohistochemistry was performed with a rabbit polyclonal anti-UCP1 antibody (1:200; ab10983, Abcam). Immunofluorescence staining was performed with a rabbit polyclonal GFP antibody (A-6455, Life Technologies). Flow cytometric analysis was performed with the following antibodies for immune profiling: CD45 (30-F11, BioLegend), F4/80 (BM8, BioLegend), CD11b (M1/70, Biolegend), MHC Class II (M5/114.15.2, BioLegend), Siglec-F (E50-2440, BD Biosciences), CD11c (N418, BioLegend), CD206 (MR5D3, BioLegend), CD3 (17A2, BioLegend; 17A2, BioLegend), TCRγδ (UC7-13D5, BioLegend), TCRβ (H57-597, BioLegend), CD4 (GK1.5, BioLegend), CD8 (53-6.7, BioLegend), CD19 (1D3/CD19, BioLegend) and B220 (Ra3-6B2, BioLegend). Intracellular analysis of ChAT expression was performed with a rabbit monoclonal ChAT antibody (ab181023, Abcam) or isotype IgG control followed by BV421-conjugated anti-rabbit secondary antibody (BioLegend).

10. Eukaryotic cell lines

a. State the source of each eukaryotic cell line used.

HEK293 cells were used in the luciferase reporter assay and is from ATCC (CRL-1573).

b. Describe the method of cell line authentication used.

The HEK293 cells have not been authenticated by our lab independently of ATCC's authentication.

c. Report whether the cell lines were tested for mycoplasma contamination.

We confirmed no mycoplasma contamination in the cells using a commercially available kit.

d. If any of the cell lines used are listed in the database of commonly misidentified cell lines maintained by ICLAC, provide a scientific rationale for their use.

HEK293 cells were used in the luciferase reporter assay based on previous published studies using HEK293 cells for high transfection efficiency.

Animals and human research participants

Policy information about studies involving animals; when reporting animal research, follow the ARRIVE guidelines

11. Description of research animals

Provide all relevant details on animals and/or animal-derived materials used in the study.

The 129SVE and Balb/c mice were purchased from Taconic Farms Inc. The Ucp1-CRE transgenic mice, the Ai14 reporter mice, C57BL/6J, ob/ob, ChATBAC-eGFP, ChATfl/fl, Vav-iCre, B6.SJL and Chrna2 knockout mice were obtained from the Jackson Laboratory (Stocks #024670, #007914, #000664, #000632, #007902, #016920, #008610, #002014 and #005797 respectively). β-less mice were provided by Brad Lowell (Beth Israel Deaconess Medical Center, Boston). All animal studies were conducted according to the protocol reviewed and approved by the University Committee on Use and Care of Animals at the University of Michigan. All mice were housed under 12-h light/12-h dark cycle (6 a.m.–6 p.m.) with a standard rodent chow diet unless otherwise specified.

Policy information about studies involving human research participants

12. Description of human research participants

Describe the covariate-relevant population characteristics of the human research participants.

Only de-identified human adipose stromal cells isolated from subcutaneous and perirenal depots were used. All specimens were collected under the protocols reviewed and approved by the Western Institutional Review Board (Puyallup, WA) or the University of Michigan Medical School Institutional Review Board (IRBMED).